APL Materials ARTICLE scitation.org/journal/apm

Photoemission electron microscopy of magneto-ionic effects in $La_{0.7}Sr_{0.3}MnO_3$

Cite as: APL Mater. 8, 111102 (2020); doi: 10.1063/5.0022150
Submitted: 17 July 2020 • Accepted: 4 October 2020 •
Published Online: 4 November 2020

Marek Wilhelm,[1,a] Margret Giesen,[1] Tomáš Duchoň,[1] Marco Moors,[1,2] David N. Mueller,[1] Johanna Hackl,[1] Christoph Baeumer,[1] Mai Hussein Hamed,[1] Lei Cao,[3,4] Hengbo Zhang,[4] Oleg Petracic,[4] Maria Glöß,[1,2,5] Stefan Cramm,[1] Slavomír Nemšák,[1,6] Carsten Wiemann,[1] Regina Dittmann,[1,5] Claus M. Schneider,[1,7,8] and Martina Müller[1,9]

AFFILIATIONS

[1]Forschungszentrum Jülich GmbH, Peter-Grünberg-Institute, 52425 Jülich, Germany
[2]Leibniz-Institute of Surface Engineering (IOM), Department of Functional Surfaces, 04318 Leipzig, Germany
[3]Institute of Ion Beam Physics and Materials Research, Helmholtz-Zentrum Dresden-Rossendorf, 01328 Dresden, Germany
[4]Jülich Centre for Neutron Science (JCNS-2), Peter-Grünberg-Institute (PGI-4), JARA-FIT, Forschungszentrum Jülich GmbH, 52425 Jülich, Germany
[5]JARA-FIT, RWTH Aachen University, 52056 Aachen, Germany
[6]Advanced Light Source, Lawrence Berkeley National Laboratory, Berkeley, California 94720, USA
[7]Faculty of Physics, University of Duisburg-Essen, 47057 Duisburg, Germany
[8]Department of Physics, UC Davis, Davis, California 95616, USA
[9]Faculty of Physics, University of Konstanz, 78457 Konstanz, Germany

Note: This paper is part of the Special Topic on Magnetoelectric Materials, Phenomena, and Devices.
[a]**Author to whom correspondence should be addressed:** m.wilhelm@fz-juelich.de

ABSTRACT

Magneto-ionic control of magnetism is a promising route toward the realization of non-volatile memory and memristive devices. Magneto-ionic oxides are particularly interesting for this purpose, exhibiting magnetic switching coupled to resistive switching, with the latter emerging as a perturbation of the oxygen vacancy concentration. Here, we report on electric-field-induced magnetic switching in a $La_{0.7}Sr_{0.3}MnO_3$ (LSMO) thin film. Correlating magnetic and chemical information via photoemission electron microscopy, we show that applying a positive voltage perpendicular to the film surface of LSMO results in the change in the valence of the Mn ions accompanied by a metal-to-insulator transition and a loss of magnetic ordering. Importantly, we demonstrate that the voltage amplitude provides granular control of the phenomena, enabling fine-tuning of the surface electronic structure. Our study provides valuable insight into the switching capabilities of LSMO that can be utilized in magneto-ionic devices.

I. INTRODUCTION

Transition metal oxides (TMOs) reveal a multitude of chemical, structural, and physical properties, such as insulating and metallic states, piezoelectricity, superconductivity, and different magnetic ordering. They can be altered by subtle distortions of the coordination environments, i.e., changes in composition, temperature, and external electric fields.[1–3] The variety inherent in TMOs stems from the complex relation between the cationic d-electron configuration and their corresponding crystal structure, which provide a multitude of electronic configurations with small energy differences.[4,5] Moreover, transition metals can appear in multiple oxidation states, which enable an electron transfer between those different cationic valencies and may stabilize a variety of magnetic states.[6]

Special attention is paid to mixed-valence $La_{0.7}Sr_{0.3}MnO_{3-\delta}$ (LSMO), a half-metallic magnetic oxide, which exhibits a large spin polarization (~95%) and the highest Curie temperature of T_C = 370 K known for the group of manganites.[7,8] Furthermore, a magnetoresistance (MR) larger than ~1800%, which has been reported,[8,9] has been widely used in magnetic oxide tunnel junction-based devices with effective spin injection behavior. As an extensively investigated magnetoelectric (ME) material, LSMO has been the subject of numerous studies revealing ME coupling via strain,[10,11] charge carrier doping,[12] and interfacial exchange processes.[13]

The strong correlation between the physical properties and the electronic- and atomic structure leads to a considerable sensitivity to ionic crystal defects and particularly oxygen vacancies.[14] The formation and dynamics of oxygen vacancies can be substantially controlled by strain,[15] temperature,[16] and external electric fields,[17] providing reversible manipulation between two or multiple states,[18] which has attracted enormous scientific and technological interest.

Recently, the field of magneto-ionics received increased attention as the voltage-driven chemical intercalation of ionic species opened a novel route toward the control of magnetism in bulk materials. One of the first studies reported about the migration of oxygen vacancies in magnetic Fe–O/Fe layers in contact with ionic liquid electrolytes, which modulated near-surface and bulk magnetism.[19] In the scope of magnetic oxides, electrolyte-gated LSMO devices showed a substantial formation and annihilation of oxygen vacancies affecting magnetic bulk properties (20 nm)[20] and providing switching capabilities for large sample areas with large spatial homogeneity and high switching speed.[21] Beyond ionic electrolyte gating also, solid–solid devices exhibit promising magneto-ionic effects. It has been shown that using strongly reducing films as a capping layer on LSMO induces significant oxygen migration and enables the control of magnetic properties. A subsequent long-time exposure to atmospheric oxygen can restore the pristine state of LSMO, and oxygen vacancies as induced by reducing capping layers are refilled with oxygen atoms.[22] Recently, a combined resistive switching experiment with a structural monitoring utilizing *in situ* transmission electron microscopy (TEM) revealed a reversible phase transition from a half-metallic and perovskite (PV) structure into an insulating and brownmillerite (BM) state.[23] Moreover, an annealing study in vacuum demonstrated a topotactic phase transition from BM to PV accompanied with a magnetic transition from antiferromagnetic to a ferromagnetic ordering and an insulator-to-metal transition.[24]

The prevalent multi-phase transition capabilities in LSMO open up valuable potential for future non-volatile memristive devices. Although, there are many reports about electric field-induced chemical and physical changes in LSMO, the driving mechanism is not completely understood and needs further investigations utilizing advanced combined probing techniques.

In this study, we employ local conductivity atomic force microscopy (AFM) and x-ray photoemission electron microscopy (PEEM) to investigate the correlation of magnetic and chemical information of electrically modified areas of LSMO thin films on a Nb:STO (100) substrate. Our data demonstrate a voltage-driven change in the Mn ion valency accompanied by a metal-to-insulator transition and a loss of magnetic ordering. The strength of the underlying microscale redox-processes can be tuned by the voltage amplitude and is reflected by significant spectral variations in the Mn $L_{3,2}$ and the O K absorption edges.

II. EXPERIMENTAL DETAILS

10 nm thick $La_{0.7}Sr_{0.3}MnO_3$ films were grown epitaxially on TiO_2-terminated Nb (0.5%):$SrTiO_3$ (100) substrates by means of pulsed laser deposition (PLD) using a 50 W KrF excimer laser at a repetition rate of 5 Hz and an energy density of 3.3 J cm^{-2}. For the film growth, the substrate was heated to a deposition temperature of 700 °C (ramping heat 50 °C/min) in an oxygen environment of p_{O_2} = 0.2 mbar. The distance between the substrate and target was set to 6 cm. In order to remove surface contaminations, the target was pre-ablated with 1800 pulses at a repetition rate of 10 Hz. After deposition, the chamber was filled with oxygen (p_{O_2} = 500 mbar) and the heater was immediately turned off. The specimen cooled down to room temperature within 1.5 h. The LSMO growth process was monitored by an *in situ* high-pressure reflection high-energy electron diffraction (RHEED) system, which confirmed a two dimensional layer-by-layer growth.

Subsequently, the morphology and the crystal structure were characterized by atomic force microscopy (AFM) and x-ray diffraction (XRD), revealing an epitaxial, single crystalline film and an atomically flat surface. Vibrating sample magnetometry (VSM) was used to investigate the saturation magnetization moment along the magnetic (110) easy axis, which amounts to $M_{Sat} = 3.4 \pm 0.34\ \mu_B$/f.u.

In preliminary experiments, we verified that the resistivity of LSMO can be changed by the application of a voltage to the surface, as shown in detail in Fig. S1. We find high (low) resistive states (HRS/LRS) in those areas where positive (negative) voltages were applied.

These pre-studies allowed us to optimize the voltage ranges for electrical modification of the samples investigated by PEEM in the following.

The electrical treatment of the pre-characterized LSMO sample was realized by utilizing local conductivity atomic force microscopy (LC-AFM) of a commercial variable temperature scanning probe microscope (VT-SPM, Scienta Omicron) equipped with a silicon ultrananocrystalline diamond (UNCD) cantilever (AppNano). The cantilever is coated with a boron-doped diamond layer and exhibits a tip radius of $R_{Tip} < 150$ nm. In order to remove any adsorbates, the sample was heated to 190 °C for about 30 min in an oxygen environment of 0.1 mbar prior to the LC-AFM measurements. The base pressure during the switching experiment was set to $3 \cdot 10^{-9}$ mbar. The electrical modification of the LSMO sample was realized by scanning over 2 × 2 μm^2 sized areas with constantly applied voltages, while the substrate was set to ground (Fig. 1). The tip scan started at one corner of the area, and the tip was moved back and forth using a total of 500 lines to cover the entire area. The scan speed was set to 5 μm/s. We wrote areas with different polarities between −3 V and +5 V. Hereinafter, we label these areas by referring to the respective voltages applied. In order to prevent unintentional modifications of the resistive states after the writing process, no read out measurements were performed afterward.

After the LC-AFM writing procedure, the samples were exposed to air and brought to the UE56-1_SGM LEEM/PEEM beamline at BESSY II, where we performed soft x-ray PEEM. All presented linearly and circularly polarized XAS-PEEM images and

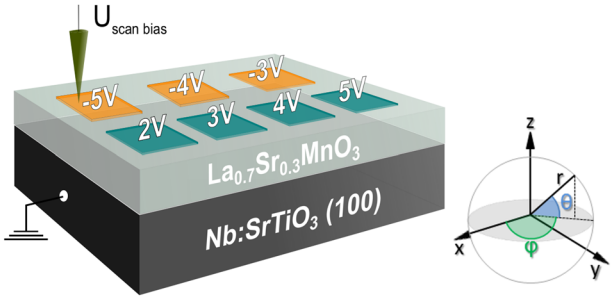

FIG. 1. Setup of the experiment in UHV: Composition stack consisting of a conducting 5 × 5 mm^2 Nb:STO (100) substrate and a 10 nm thick $La_{0.7}Sr_{0.3}MnO_3$ thin film. 2 × 2 μm^2 sized squares are written by a scanning LC-AFM tip electrode under applied constant voltages.

spectra were recorded in the total electron yield (TEY) mode and in the same field of view (20 μm). X-ray magnetic circular dichroism (XMCD) measurements were performed at room temperature and across the Mn $L_{3,2}$-edge (630 eV–670 eV) at a fixed angle of $\theta = 20°$ between the beam axis and the surface plane of the specimen. As no external magnetic field was applied during the spectromicroscopical analysis, the XMCD spectra reflect a remanent ferromagnetic response. We did not observe any magnetic inhomogeneities for the LSMO sample. Hence, the pristine LSMO sample is assumed to be in a single domain state or in an anisotropic multidomain state with a sufficiently large net magnetization and a domain size below the resolution of our PEEM measurement (~100 nm). Therefore, we conclude that the magnetic contrast as observed in our experiments is related to the electrical treatment.

III. RESULTS AND DISCUSSION

A. Photoemission electron microscopy (PEEM)

To study the micro-scale redox processes present in the electrically modified areas of the LSMO thin film, we performed x-ray photoemission electron microscopy (PEEM). PEEM provides the capability of measuring all voltage-treated areas at the same time. This allows us to directly compare magnetic and chemical properties with the electrical pre-treatment and set them into relation, since one does not have to deal with homogeneity issues and sample preparation reproducibility. The respective images and spectra were recorded for the Mn $L_{3,2}$ and O K-edges. Subsequently, we performed principle component analysis (PCA)[25,26] on the PEEM data. In PCA, the original dataset is described in a new orthogonal coordinate system, which is spanned along new principal component (PC) axes. The PCs are oriented along the largest, uncorrelated variances in the data. Spectral information is covered by the largest data variances, whereas smaller variances are generally related to noise. Hence, only a small number of PCs is sufficient to describe the relevant spectral features, and one can reconstruct the original data using merely the small set of relevant PCs, thereby improving the signal-to-noise ratio substantially. As has been demonstrated in Refs. 27 and 28, PCA can reveal small signals mostly camouflaged by noise. A further advantage of PCA is that the data variances can be related to certain pixels in the original PEEM image, thereby providing a high spatial chemical resolution. A detailed description of the principal components and the respective PEEM data reconstructions for various photon energies of the absorption edges can be found in Figs. S2–S4.

Figure 2(a) shows the PCA reconstruction of the original PEEM image for the Mn L-edge ($h\nu$ = 642.2 eV). The contrast of the areas modified with positive voltages raises with increasing amplitude and shows a significant chemical transition between 3 V and 4 V. From the previous resistive switching experiment shown in Fig. S1, we conclude that there is also a metal-to-insulator transition between 3 V and 4 V. Thus, there is an obvious correlation between the enhanced chemical contrast and the transition from pristine low resistivity to high resistivity. The areas written with a negative voltage reveal only weak contrast levels without any obvious trend.

For the cluster image and the corresponding spectra shown in Figs. 2(b) and 3–5, respectively, we made use of a cluster analysis, which is based on *ortho*-non-negative matrix factorization (*o*-NMF) and group classification of similar Euclidian distance, as described in Ref. 29. In the work presented here, *o*-NMF identifies pixel groups where PEEM spectra are similar: chemical inhomogeneities cause spectral changes that lead to mean-square deviations between spectra. The *o*-NMF identifies those deviations and sorts spectra into different groups, which are visualized in Fig. 2(b) as differently colored pixels.

In the case of voltage-treated LSMO, four clusters with sufficient spectral resolution and the most physical sense (gray, blue, red, and green) are identified for the Mn L and O K-edges. The gray cluster corresponds to untreated sample regions and represents the pristine state. Isolated, scattered blue pixels seem to be located mainly within areas treated with negative voltage. While the gray cluster can be ascribed to a fully stoichiometric $La_{0.7}Sr_{0.3}MnO_3$ thin film, the blue cluster indicates a partially reduced state. Between −5 V and −3 V, increasing the voltage leads to a slight increase in the contribution of the blue cluster. However, this increase is hardly above the noise level. It has been shown that LSMO thin films initially tend

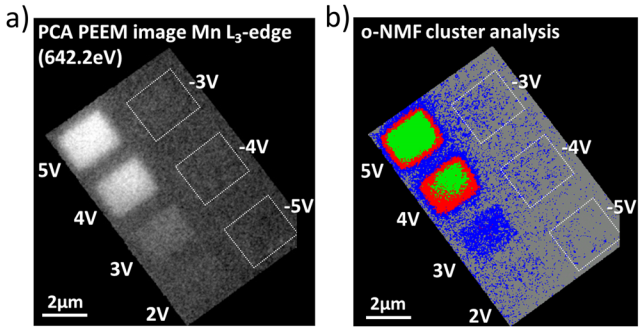

FIG. 2. Real space imaging of the Mn L_3-edge. (a) Reconstruction of the original PEEM image by the main principle components. The chemical contrast of the modified regions at the Mn L_3-edge ($h\nu$ = 642.2 eV) reveals a significantly enhanced intensity for 4 V and 5 V (HRS). (b) False-color representation of the PCA PEEM image in (a) indicating pixels of high spectral similarity as obtained by orthogonal non-negative matrix factorization (*o*-NMF). The mean spectra determined from the average over all spectra within the colored areas (gray, blue, red, and green) are plotted in Figs. 3 and 4 (top) using the same color code.

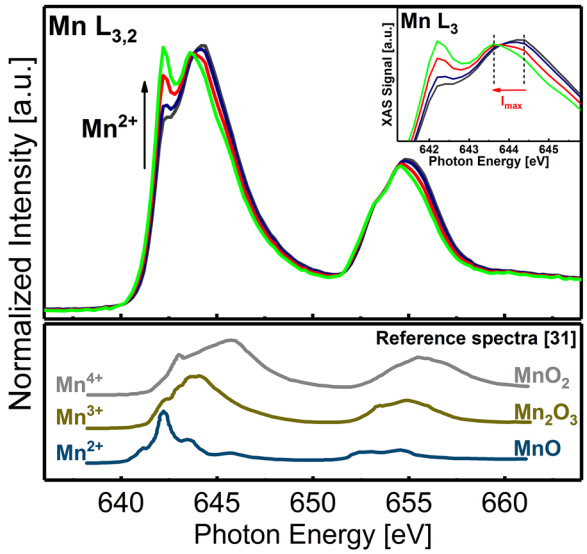

FIG. 3. Top panel: x-ray absorption spectra of the Mn $L_{3,2}$-edge averaged over the cluster regions, as shown in Fig. 2(b) using the same color code. The areas modified with a positive tip polarization show an increasing Mn^{2+} contribution with increasing voltage. Bottom panel: reference spectra indicating Mn^{2+}, Mn^{3+}, and Mn^{4+}. Adapted from Ref. 31.

to show a certain Mn^{2+} contribution at the surface[30] due to symmetry breaking effects, which could explain the observed scattered blue pixels. Hence, we conclude that the application of a negative tip bias does not significantly affect the oxidation state, since the pristine state is already in a conductive and an oxygen saturated state.

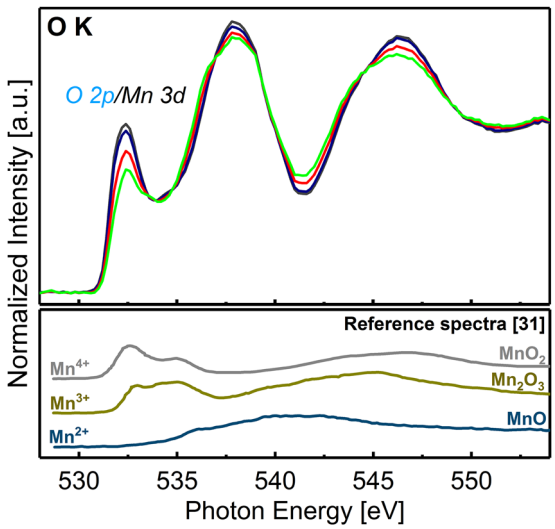

FIG. 4. Top panel: x-ray absorption spectra of the O K-edge averaged over the cluster regions, as shown in Fig. 2(b) using the same color code. The areas modified with a positive voltage reveal a decreased O 2*p*–Mn 3*d* hybridization peak with increasing voltage. Bottom panel: reference spectra indicating Mn^{2+}, Mn^{3+}, and Mn^{4+}. Adapted from Ref. 31.

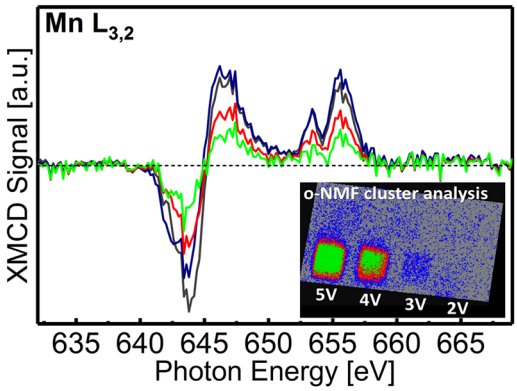

FIG. 5. XMCD spectra of the Mn $L_{3,2}$-edge extracted and averaged over the color-coded cluster regions defined by the *o*-NMF analysis (inset). The XMCD signal decreases with increasing positive voltage and reveals a significant ferromagnetic contrast between 3 V and 4 V.

The chemical contrast significantly changes between 2 V and 5 V. The area treated with 3 V shows a homogeneously distributed contribution of the blue cluster. The 4 V area consists of three clusters, which form a concentrical alignment of rectangles. From the outermost region to the center, the clusters are encoded in blue, red, and green, respectively. In the case of 5 V, we observe a similar concentrical arrangement of clusters, but with a significantly larger contribution of green in the center.

Figure 3 shows a direct comparison of the according spectra recorded at the Mn $L_{3,2}$-edge, where each color is assigned to the respective cluster as defined in the *o*-NMF analysis [Fig. 2(b)]. We observe an emerging low energy peak at $h\nu$ = 642.2 eV from gray (stoichiometric $La_{0.7}Sr_{0.3}MnO_3$) to green. A significant increase in the peak is obtained between the blue and the red spectrum, noticing that this accompanies the metal-to-insulator transition. The low energy feature that is separated by 1 eV from the main peak can be ascribed to the appearance of Mn^{2+} cations.[30,32] We also note that the main peak of the red spectrum and green spectrum, located at $h\nu$ = 644 eV, reveals an apparent shift of the maximum intensity I_{max} toward lower photon energy [see the inset of Fig. 3]. The Mn L-edges of MnO, Mn_2O_3, and MnO_2 reference samples are shown in Fig. 3. They indicate the three valence states of Mn^{2+}, Mn^{3+}, and Mn^{4+}[31] and illustrate the possible components, which might form the Mn $L_{3,2}$-edge spectra of a LSMO thin film after voltage treatment. In particular, the MnO reference spectrum illustrates the origin of the low energy peak of the measured spectra at $h\nu$ = 642.2 eV, which is assigned to Mn^{2+}. The arising Mn^{2+} contribution is a consequence of oxygen vacancies, whose concentration increases with increasing positive voltage. Applying a positive voltage induces a migration of the negatively charged oxygen ions to the surface. Subsequently, a surface exchange process leads to the release of the oxygen, which is driven by the gradient of the chemical potential of oxygen across the LSMO/vacuum interface.[33] The exchange process of the oxygen leads to a significant valence change from a $Mn^{3+/4+}$ to a $Mn^{2+/3+}$ dominated state.

The concentrical alignment of the clusters, shown in Fig. 2(b), is likely caused by the gradient of the applied field, the scanning

pattern, and the scanning speed. The difference in exposure to the electric field is known to influence magneto-ionic effects.[34]

A variation of the oxygen vacancy concentration should also impact the O K-edge spectra (Fig. 4), particularly on the peak located at $h\nu = 532.3$ eV, which is assigned to the hybridization state between the O 2*p* and the Mn 3*d* states.[35,36] As it is obvious from the reference spectra in Fig. 4 (bottom), a decrease in the oxidation state of the Mn leads to a decrease in the O 2*p*–Mn 3*d* hybridization peak.

The gray spectrum reveals the largest intensity as it represents the oxygen saturated pristine LSMO thin film. The peak intensity decreases from blue to green, indicating less unoccupied electronic states of the manganese and corroborating the increasing oxygen vacancy concentration for increasing positive voltages. In line with the metal-to-insulator transition and the results from the Mn L-edge, we observe a considerable modification of the spectral intensities between the blue spectrum and the red spectrum. Our observations of significant changes in the manganese valence state, the incorporation of oxygen vacancies, and the metal-to-insulator transition already strongly suggest that the magnetic properties may very likely be affected due to a diminished double exchange coupling.

B. X-ray magnetic circular dichroism

In order to gain a deeper understanding of the electrically induced change in the magnetic properties and altered exchange interactions, spin-sensitive and element-selective XMCD-PEEM measurements of the Mn $L_{3,2}$-edge will scrutinize the interplay between valence change, resistivity, and magnetic ordering.

The XMCD signals of each cluster exhibit the characteristic ferromagnetic signature of perovskite LSMO thin films at room temperature,[37,38] which originates from the double exchange interaction between Mn^{3+} and Mn^{4+}. The gray XMCD spectrum reveals the largest XMCD signal and represents the pristine ferromagnetic state. The strength of the XMCD signal decreases with increasing positive voltage. From this, we deduce a clear dependence of the ferromagnetic properties on the oxygen vacancy concentration and the corresponding Mn valence state. A straightforward explanation for this phenomenon is a disturbed double exchange interaction, which has two reasons: In LSMO, with a Sr doping concentration of 30%, oxygen vacancies act as electron donors (causing a valence change in order to preserve charge neutrality), weakening the double exchange interaction and promoting antiferromagnetic coupling. Moreover, the delocalization of the e_g electron between the Mn^{3+} and Mn^{4+} cations is crucial in order to stabilize a parallel and ferromagnetic alignment of the respective t_{2g} electron spin states. Since the delocalization of the e_g electron is mediated by an interlinking oxygen anion between Mn^{3+} and Mn^{4+}, the exchange process is perturbated due to a missing oxygen anion. Thus, an increasing concentration of oxygen vacancies leads to a gradual transition from a ferromagnetic through antiferromagnetic to a nonmagnetic state.

Besides a perturbation of the driving double exchange mechanism, there could be other explanations for the decreasing ferromagnetic signal. For example, recent studies on LSMO reported on a structural phase transition from a perovskite (PV) ABO_3 to a brownmillerite (BM) $ABO_{2.5}$ structure driven by the application of an electric field to the thin film surface[23] and by an annealing procedure in vacuum.[24] The latter study also revealed a concomitant magnetic phase transition from a ferromagnetic (PV) to an antiferromagnetic ordering (BM) with a Néel temperature of $T_N = 30$ K and a paramagnetic state at room temperature. Thus, we performed XAS also on a BM reference sample, which is discussed in the supplementary material (see Fig. S8). While the XMCD results could support the picture of an existing BM phase in the HRS, the absorption spectra are not evidential. The green and red spectra at the Mn $L_{3,2}$-edge (Fig. 3) would corroborate a BM phase. The spectra we find for the green and red cluster at the O K-edge (Fig. 4), however, are not consistent with the reference spectra for BM (Fig. S8), rendering it unlikely that the HRS state corresponds to the BM phase. For clarification, a complementary analysis of the modified regions by transmission electron microscopy may unveil possible BM structures and will be part of our future investigation. Under well-chosen experimental conditions (proper thickness of the cut lamella and probing the right crystal orientation), prevalent BM phases embedded in a perovskite matrix could provide sufficient transmission contrasts in order to identify respective filaments.[23]

IV. CONCLUSION

We performed a combined element selective and spatially resolved XAS and XMCD study of electrically modified areas in $La_{0.7}Sr_{0.3}MnO_3$ thin films. Our results demonstrate the direct interplay between resistivity, chemical composition, and magnetic ordering driven by an oxygen exchange process across the LSMO film surface. Significant chemical modifications are observed in the high resistive state, where the incorporation of oxygen vacancies leads to a distinct valence change from $Mn^{3+/4+}$ to $Mn^{2+/3+}$. Furthermore, a direct correlation between oxygen deficiency and a degradation of the ferromagnetic properties is found.

In this light, these results provide novel insight into the vacancy-driven magneto-ionic control of magnetoelectric oxides. Moreover, they open up novel routes toward a multiphase-control of physical and chemical properties in complex oxides and novel ionotronic devices.

SUPPLEMENTARY MATERIAL

See the supplementary material for a discussion of the electronic properties, a detailed description of the principal component analysis, information about the XMCD analysis, and a comparison of the brownmillerite and perovskite x-ray absorption fingerprints.

ACKNOWLEDGMENTS

This work was funded by the Deutsche Forschungsgemeinschaft (DFG) within the Grant No. SFB 917. M. Glöß acknowledges for the support from the Emmy Noether program of the DFG.

DATA AVAILABILITY

The data that support the findings of this study are available within the article and its supplementary material.

REFERENCES

[1] S. V. Kalinin and N. A. Spaldin, "Functional ion defects in transition metal oxides," Science **341**, 858–859 (2013).
[2] M. A. Peña and J. L. G. Fierro, "Chemical structures and performance of perovskite oxides," Chem. Rev. **101**, 1981–2018 (2001).

[3]S. Stølen, E. Bakken, and C. E. Mohn, "Oxygen-deficient perovskites: Linking structure, energetics and ion transport," Phys. Chem. Chem. Phys. **8**, 429–447 (2006).
[4]N. Hamada, H. Sawada, I. Solovyev, and K. Terakura, "Electronic band structure and lattice distortion in perovskite transition-metal oxides," Physica B **237-238**, 11–13 (1997).
[5]J. Chakhalian, J. W. Freeland, A. J. Millis, C. Panagopoulos, and J. M. Rondinelli, "Colloquium: Emergent properties in plane view: Strong correlations at oxide interfaces," Rev. Mod. Phys. **86**, 1189–1202 (2014).
[6]C. N. R. Rao, "Transition metal oxides," Annu. Rev. Phys. Chem. **40**, 291–326 (1989).
[7]M. Bowen, M. Bibes, A. Barthélémy, J.-P. Contour, A. Anane, Y. Lemaître, and A. Fert, "Nearly total spin polarization in $La_{2/3}Sr_{1/3}MnO_3$ from tunneling experiments," Appl. Phys. Lett. **82**, 233–235 (2003).
[8]A. Urushibara, Y. Moritomo, T. Arima, A. Asamitsu, G. Kido, and Y. Tokura, "Insulator-metal transition and giant magnetoresistance in $La_{1-x}Sr_xMnO_3$," Phys. Rev. B **51**, 14103–14109 (1995).
[9]A. Thomas, S. Niehörster, S. Fabretti, N. Shepheard, O. Kuschel, K. Küpper, J. Wollschläger, P. Krzysteczko, and E. Chicca, "Tunnel junction based memristors as artificial synapses," Front. Neurosci. **9**, 241 (2015).
[10]S. K. Chaluvadi, F. Ajejas, P. Orgiani, S. Lebargy, A. Minj, S. Flament, J. Camarero, P. Perna, and L. Méchin, "Epitaxial strain and thickness dependent structural, electrical and magnetic properties of $La_{0.67}Sr_{0.33}MnO_3$ films," J. Phys. D: Appl. Phys. **53**, 375005 (2020).
[11]W. Eerenstein, M. Wiora, J. L. Prieto, J. F. Scott, and N. D. Mathur, "Giant sharp and persistent converse magnetoelectric effects in multiferroic epitaxial heterostructures," Nat. Mater. **6**, 348–351 (2007).
[12]A. Molinari, P. M. Leufke, C. Reitz, S. Dasgupta, R. Witte, R. Kruk, and H. Hahn, "Hybrid supercapacitors for reversible control of magnetism," Nat. Commun. **8**, 15339 (2017).
[13]P. Zhou, K. Liang, Y. Liu, Z. Zheng, and T. Zhang, "Effect of interface coupling on magnetoelectric response of $Pb(Zr_{0.52}Ti_{0.48})O_3/La_{0.67}Sr_{0.33}MnO_3$ thin film under different strain states," Appl. Phys. A **124**, 670 (2018).
[14]S. B. Adler, "Chemical expansivity of electrochemical ceramics," J. Am. Ceram. Soc. **84**, 2117–2119 (2001).
[15]J. R. Petrie, C. Mitra, H. Jeen, W. S. Choi, T. L. Meyer, F. A. Reboredo, J. W. Freeland, G. Eres, and H. N. Lee, "Strain control of oxygen vacancies in epitaxial strontium cobaltite films," Adv. Funct. Mater. **26**, 1564–1570 (2016).
[16]J. Wu, J. Wang, D. Xiao, and J. Zhu, "Migration kinetics of oxygen vacancies in Mn-modified $BiFeO_3$ thin films," ACS Appl. Mater. Interfaces **3**, 2504–2511 (2011).
[17]D. A. Gilbert, A. J. Grutter, P. D. Murray, R. V. Chopdekar, A. M. Kane, A. L. Ionin, M. S. Lee, S. R. Spurgeon, B. J. Kirby, B. B. Maranville *et al.*, "Ionic tuning of cobaltites at the nanoscale," Phys. Rev. Mater. **2** (2018).
[18]N. Lu, P. Zhang, Q. Zhang, R. Qiao, Q. He, H.-B. Li, Y. Wang, J. Guo, D. Zhang, Z. Duan, Z. Li, M. Wang, S. Yang, M. Yan, E. Arenholz, S. Zhou, W. Yang, L. Gu, C.-W. Nan, J. Wu, Y. Tokura, and P. Yu, "Electric-field control of tri-state phase transformation with a selective dual-ion switch," Nature **546**, 124–128 (2017).
[19]K. Duschek, D. Pohl, S. Fähler, K. Nielsch, and K. Leistner, "Research update: Magnetoionic control of magnetization and anisotropy in layered oxide/metal heterostructures," APL Mater. **4**, 032301 (2016).
[20]B. Cui, C. Song, G. Wang, Y. Yan, J. Peng, J. Miao, H. Mao, F. Li, C. Chen, F. Zeng, and F. Pan, "Reversible ferromagnetic phase transition in electrode-gated manganites," Adv. Funct. Mater. **24**, 7233–7240 (2014).
[21]A. Molinari, H. Hahn, and R. Kruk, "Voltage-controlled on/off switching of ferromagnetism in manganite supercapacitors," Adv. Mater. **30**, 1703908 (2018).
[22]A. J. Grutter, D. A. Gilbert, U. S. Alaan, E. Arenholz, B. B. Maranville, J. A. Borchers, Y. Suzuki, K. Liu, and B. J. Kirby, "Reversible control of magnetism in $La_{0.67}Sr_{0.33}MnO_3$ through chemically-induced oxygen migration," Appl. Phys. Lett. **108**, 082405 (2016).
[23]L. Yao, S. Inkinen, and S. van Dijken, "Direct observation of oxygen vacancy-driven structural and resistive phase transitions in $La_{2/3}Sr_{1/3}MnO_3$," Nat. Commun. **8**, 14544 (2017).
[24]L. Cao, O. Petracic, P. Zakalek, A. Weber, U. Rücker, J. Schubert, A. Koutsioubas, S. Mattauch, and T. Brückel, "Reversible control of physical properties via an oxygen-vacancy-driven topotactic transition in epitaxial $La_{0.7}Sr_{0.3}MnO_{3-\delta}$ thin films," Adv. Mater. **31**, 1806183 (2019).
[25]I. Jolliffe, "Principal components in regression analysis," in *Principal Component Analysis* (Springer, 1986).
[26]J. Jackson, *A User's Guide to Principal Components* (Frontiers in Neuroscience, 2004).
[27]M. Giesen, M. Jugovac, G. Zamborlini, V. Feyer, F. Gunkel, and D. N. Mueller, "Principal component analysis: Reveal camouflaged information in x-ray absorption spectroscopy photoemission electron microscopy of complex thin oxide films," Thin Solid Films **665**, 75–84 (2018).
[28]D. Stadler, D. N. Mueller, T. Brede, T. Duchoň, T. Fischer, A. Sarkar, M. Giesen, C. M. Schneider, C. A. Volkert, and S. Mathur, "Magnetic field-assisted chemical vapor deposition of iron oxide thin films: Influence of field-matter interactions on phase composition and morphology," J. Phys. Chem. Lett. **10**, 6253–6259 (2019).
[29]A. Mirzal, "A convergent algorithm for orthogonal nonnegative matrix factorization," J. Comput. Appl. Math. **260**, 149–166 (2014).
[30]M. P. de Jong, I. Bergenti, V. A. Dediu, M. Fahlman, M. Marsi, and C. Taliani, "Evidence for Mn^{2+} ions at surfaces of $La_{0.7}Sr_{0.3}MnO_3$ thin films," Phys. Rev. B **71**, 014434 (2005).
[31]R. Qiao, T. Chin, S. J. Harris, S. Yan, and W. Yang, "Spectroscopic fingerprints of valence and spin states in manganese oxides and fluorides," Curr. Appl. Phys. **13**, 544–548 (2013).
[32]G. van der Laan and I. W. Kirkman, "The 2p absorption spectra of 3d transition metal compounds in tetrahedral and octahedral symmetry," J. Phys.: Condens. Matter **4**, 4189–4204 (1992).
[33]J. Fleig, H.-R. Kim, J. Jamnik, and J. Maier, "Oxygen reduction kinetics of lanthanum manganite (LSM) model cathodes: Partial pressure dependence and rate-limiting steps," Fuel Cells **8**, 330–337 (2008).
[34]A. Quintana, E. Menéndez, M. O. Liedke, M. Butterling, A. Wagner, V. Sireus, P. Torruella, S. Estradé, F. Peiró, J. Dendooven, C. Detavernier, P. D. Murray, D. A. Gilbert, K. Liu, E. Pellicer, J. Nogues, and J. Sort, "Voltage-controlled ON–OFF ferromagnetism at room temperature in a single metal oxide film," ACS Nano **12**, 10291–10300 (2018).
[35]B. Cui, C. Song, F. Li, G. Y. Wang, H. J. Mao, J. J. Peng, F. Zeng, and F. Pan, "Tuning the entanglement between orbital reconstruction and charge transfer at a film surface," Sci. Rep. **4**, 4206 (2014).
[36]L. Piper, A. Preston, S. Cho, A. Demasi, B. Chen, J. Laverock, K. Smith, L. Miara, J. Davis, S. Basu, U. Pal, S. Gopalan, L. Saraf, T. Kaspar, A. Matsuura, P. Glans, and J. Guo, "Erratum: Soft x-ray spectroscopic study of dense strontium-doped lanthanum manganite cathodes for solid oxide fuel cell applications [J. Electrochem. Soc., 158, B99 (2011)]," J. Electrochem. Soc. **158**, S9(2011).
[37]J.-S. Lee, C.-C. Kao, T. S. Santos, E. Negusse, and D. A. Arena, "Reversed remanent magnetic configuration in epitaxial $La_{1-x}Sr_xMnO_3$films," J. Phys. D: Appl. Phys. **44**, 245002 (2011).
[38]T. Taniuchi, H. Kumigashira, M. Oshima, T. Wakita, T. Yokoya, M. Kubota, K. Ono, H. Akinaga, M. Lippmaa, M. Kawasaki, and H. Koinuma, "Observation of step-induced magnetic domain formation in $La_{1-x}Sr_xMnO_3$ thin films by photoelectron emission microscopy," Appl. Phys. Lett. **89**, 112505 (2006).